PAPER

Effect of the frequency chirp on laser wakefield acceleration

To cite this article: V B Pathak *et al* 2012 *New J. Phys.* **14** 023057

View the article online for updates and enhancements.

New Journal of Physics

Effect of the frequency chirp on laser wakefield acceleration

V B Pathak[1,3], J Vieira[1], R A Fonseca[1,2] and L O Silva[1]

[1] GoLP/Instituto de Plasmas e Fusão Nuclear-Laboratório Associado, Instituto Superior Técnico, 1049-001 Lisboa, Portugal
[2] DCTI/ISCTE Lisbon University Institute, 1649-026 Lisbon, Portugal
E-mail: vishwa.bandhu@ist.utl.pt

Abstract. The role of laser frequency chirps in the laser wakefield accelerator is examined. We show that in the linear regime, the evolution of the laser pulse length is affected by the frequency chirp, and that positive (negative) chirp compresses (stretches) the laser pulse, thereby increasing (decreasing) the peak vector potential and wakefield amplitude. In the blowout regime, the frequency chirp can be used to fine-tune the localized etching rates at the front of the laser. In our simulations, chirped laser pulses can lead to 15% higher self-trapped electrons and 10% higher peak energies as compared to the transform-limited pulse. Chirps may be used to control the phase velocity of the wake and to relax the self-guiding conditions at the front of the laser. Our predictions are confirmed by multi-dimensional particle-in-cell simulations with OSIRIS.

Contents

[3] Author to whom any correspondence should be addressed.

1. Introduction

One of the main goals of plasma-based accelerators is to deliver multi-GeV electrons [1–4] at distances that can be orders of magnitude shorter than those with standard acceleration techniques. Recent particle-in-cell (PIC) simulations in Lorentz-boosted frames [4, 5] predict electron bunch energies beyond 10 GeV in meter-scale plasmas using next-generation 10 petawatt laser systems. In fact, accelerating wakefields of nearly 50 GeV m^{-1} have been observed experimentally in plasmas [1], which are almost 1000 times higher than the fields observed in conventional accelerators. In laser or plasma wakefield acceleration (LWFA/PWFA), a short laser pulse or ultra-relativistic electron beam propagates in an underdense plasma, and excites plasma waves [6, 7] that can trap and accelerate electrons to ultra-relativistic energies. This paper examines the role of the frequency chirped laser in LWFA, where the laser pushes plasma electrons away from the propagation axis through the ponderomotive force. This creates a positive space charge, as the ions remain essentially immobile on the time scales associated with the plasma period. Depending upon the laser and plasma parameters, linear or nonlinear plasma waves are excited. If the laser intensity is sufficiently high, the radial ponderomotive force can lead to the cavitation of all the plasma electrons from the region where the laser propagates, creating a spherical plasma wave (bubble or blowout regime [8, 9]).

The potential of the blowout regime for several applications has been confirmed in numerous experiments. The large accelerating fields associated with the blowout, which can trap and accelerate plasma electrons (self-injection), lead to the generation of quasi-monoenergetic multi-GeV electrons [2, 3, 10–12]. In addition, the linear transverse focusing forces associated with the bubble [9] are ideal for the generation of x-ray radiation, as the accelerated electron beams perform betatron oscillations in the ion channel [13–16]. The beams obtained from LWFA also have potential to drive a free electron laser [17] after solving their present beam quality issues. For these applications it is crucial to control and manipulate the injection process that determines the charge, energy, energy spread and strength parameter for x-ray radiation [18]. Although several techniques have been proposed for this purpose, including the use of short plasma down-ramps [19, 20], the use of transverse external magnetic fields [21], and through the beating structures associated with counter or cross-propagating lasers [2, 22, 23] and through ionization mechanisms [24], this paper explores the possibility of using chirped lasers to control self-injection.

Previous investigations of the role of the laser envelope asymmetries in wakefield excitation have already shown that a sharp laser intensity rise can drive stronger wakefields [25–27]. In addition, theoretical and simulation works [28, 29] on the impact of frequency chirps on the long pulse instabilities have shown that the growth of Raman forward scattering-like instabilities can be controlled by acting upon the laser frequency chirps. The role of frequency chirps in the laser intensity profile has been explored experimentally [30] in the self-modulated LWFA, showing significant enhancement of the total charge for sharp rising asymmetric pulses with positive chirps, where the frequency is lower at the front of the laser pulse. In this case, the ponderomotive force is also stronger at the front of the laser, which leads to stronger wakefields. Supported by analytical results, these experiments then emphasized the importance of the asymmetry of the laser pulse for the wake excitation and particle acceleration.

In this paper, we investigate, through numerical simulations with two-dimensional (2D) and 3D PIC simulations in OSIRIS [31], the role of the frequency chirps in the blowout regime

to show that the chirp can be used to adjust the self-injection rates, charge and the output energy of LWFA. For the same plasma density, even though the peak energy of the accelerated electrons is at the same level for the chirped and un-chirped laser pulses, the total injected charge can be increased by 15%, using a chirped pulse laser for these parameters. Positive chirps increase (decrease) the self-injected charge (maximum energy) by up to 10% in comparison to negative chirps in state-of-the-art conditions. Moreover, frequency chirps also change the laser group velocity in the plasma. These results agree with [30], although they are due to a different physical mechanism.

In section 2, an analytical model for the longitudinal bunching of a laser pulse with a frequency chirp is developed in the linear regime. Our model shows that laser with positive (negative) frequency chirp will compress (stretch) throughout the propagation. Accordingly, in the linear regime positive (negative) chirp leads to higher (lower) peak laser intensities. Good agreement between the analytical model and the simulations is observed in the linear regime. In section 3, the evolution of the linear wake is investigated for different frequency chirped driving laser pulses. Although initially the wakefield amplitude is nearly independent of the sign of the frequency chirp, at later stages of the laser propagation, the wakefield amplitude increases (decreases) for positively (negatively) chirped pulse. In the blowout regime, which cannot be examined by the linear model, the peak intensity increases for positive as well as negative chirps; however, the positively chirped pulse evolves faster than the negatively chirped pulse. In section 4, the effect of frequency chirp on self-injection in the blowout regime is analyzed. Finally, the conclusions are stated in section 5.

2. Longitudinal bunching

The dominant contributions to the plasma refractive index, associated with the propagation of short laser pulses, come from the ponderomotive and effective mass nonlinearities. The nonlinear coupling between the laser pulse and the plasma dynamics can lead to several processes, such as laser self-steepening [27], self-compression [32], self-focusing [33] and self-modulation ([7, 33] and references therein). For our work, however, the most relevant mechanisms are associated with the self-compression, by which the laser pulse length changes during its propagation in the plasma.

In order to examine the self-compression of a chirped laser pulse, we will use similar physical arguments to those presented in [33]. Our analysis is valid as long as the envelope approximation can be employed, i.e. as long as $k_0 L_0 \gg 1$, where k_0 is the central laser wave number and L_0 is the laser pulse length. This assumption is well verified in the LWFA, where the refractive index for a linearly polarized laser pulse, in the weakly relativistic regime, becomes [33]

$$\eta = \left[1 - \frac{\omega_p^2}{2\omega_0^2} \left\{ 1 + \frac{\delta n}{n_0} - \frac{\langle a^2 \rangle}{2} - 2\frac{\delta\omega}{\omega_0} \right\} \right], \tag{1}$$

where $\omega_p = \sqrt{n_0 e^2/(m\epsilon_0)}$ is the plasma frequency, n_0 is the background plasma density, ω_0 is the laser frequency, $a = eA/(m_e c^2)$ is the normalized vector potential, m_e is the electron mass and c is the speed of light, and where $\delta n = n - n_0$ and $\delta\omega = \omega - \omega_0$ are perturbations to the plasma density and laser central frequency ω_0. In addition, $\langle a^2 \rangle$ is the average of a^2 over one laser period. According to equation (1), the laser group velocity of the laser

$v_g = (c^2/v_\phi)/[1 + \omega_p^2(\gamma_0 - 1)/(2\omega_0^2\gamma_0(\gamma_0 + 1))]$ [33, 34], where $v_\phi = c\eta^{-1}$ is the phase velocity and $\gamma_0 = \sqrt{(1 + \langle a^2 \rangle/2)}$, can be written as [33]

$$v_g = c\left[1 - \frac{\omega_p^2}{2\omega_0^2}\left\{1 + \frac{\delta n}{n_0} - \frac{\langle a^2 \rangle}{4} - 2\frac{\delta\omega}{\omega_0}\right\}\right]. \tag{2}$$

In equations (1) and (2), the second term within the braces ({}) is related to the plasma density perturbations δn, the next term represents the relativistic effects associated with the quiver motion of the electrons in the laser field, and the last term is due to the laser frequency modulations. The evolution of the laser pulse length is given by [33]

$$\frac{1}{L}\frac{\partial L}{\partial t} = -\frac{1}{c}\frac{\partial v_g}{\partial \xi}, \tag{3}$$

where L is the laser length, t is time, and $\xi = t - z/c$ is the distance in the co-moving frame. Using equation (2), equation (3) can be rewritten as

$$\frac{\partial \log L}{\partial t} = \frac{\omega_p^2}{2\omega_0^2}\frac{\partial}{\partial \xi}\left[\frac{\delta n}{n_0} - \frac{\langle a^2 \rangle}{4} - 2\frac{\delta\omega}{\omega_0}\right]. \tag{4}$$

To examine the relative contributions of these terms, we can consider, in the linear regime, the laser pulse profile $\langle a^2 \rangle \sim a_0^2 \sin^2(c\pi\xi/L)$. For this profile, the density modulation in the wake varies as $\delta n/n_0 \sim \pi a_0^2 \sin(\omega_p\xi)/8$ [7] and the maximum contribution from the first two terms on the right-hand side of equation (4) is $\sim \omega_p a_0^2/2$. In the regime where $\delta\omega/\omega_0 \gg \omega_p a_0^2/4$, the effect of ponderomotive and relativistic nonlinearities can be neglected with respect to the term for the spectrum change. In an underdense plasma ($\omega_p^2/\omega_0^2 \ll 1$), for a Gaussian chirped laser pulse with electric field $\vec{E} = \vec{E}_0 \exp(-c^2\xi^2/L^2)\exp(-i\omega_0(1 + \beta\xi)\xi)$ and chirp coefficient β, the average wave number $\langle k \rangle = \int_{-\infty}^{\infty} k\mathcal{W}(d)k/(\int_{-\infty}^{\infty}\mathcal{W}dk)$ [35, 36], where $\mathcal{W} = \int ds\,\vec{E}(\xi - s/2)\cdot\vec{E}^*(\xi + s/2)\exp(iks)$ is the Wigner transform, can be written as $\langle k \rangle = k_0(1 + 2\beta\xi)$, with $k_0 \approx \omega_0$ and $\delta\omega/\omega_0 \approx \delta\langle k \rangle/k_0 = 2\beta\xi$. Therefore, the first and second terms on the right-hand side of equation (4) can be neglected when $2\beta\xi \sim 2\beta L \gg \omega_p a_0^2/L$. In the remainder of this paper, $\beta \gg \omega_p a_0^2/2$ will be assumed.

To evaluate further equation (4), we note that in the absence of any nonlinear plasma effects, the frequency chirp coefficient of a Gaussian chirped pulse varies as $\beta = [2c^2 \ln 2/(L^2\omega_0)]\sqrt{(L/L_{in})^2 - 1}$ [37], where L_{in} is the pulse length of the transform-limited laser pulse. As the laser pulse disperses with time, the rate of frequency variation inside the pulse changes, and the frequency chirp coefficient varies as $\beta = \beta_0(L_0/L)^2$ $\sqrt{(L^2 - L_{in}^2)/(L_0^2 - L_{in}^2)}$, where L_0 and β_0 are the initial pulse length and the frequency chirp coefficient respectively. For $L, L_0 \gg L_{in}$, the frequency chirp coefficient varies as $\beta = \beta_0 L_0/L$. Equation (4) then yields

$$L = L_0\left[\left(1 - \frac{L_{in}^2}{L_0^2}\right)\left(1 - 2\beta_0 t\frac{\omega_p^2}{\omega_0^2}\frac{1}{1 - L_{in}^2/L_0^2}\right)^2 + \frac{L_{in}^2}{L_0^2}\right]^{1/2}, \tag{5}$$

where $L_{in}/L_0 = \sqrt{1/[1 + (L_0^2\omega_0\beta_0)^2/(2c^2 \ln 2)^2]}$. For the typical parameters of interest for LWFA ($L_0 \sim \lambda_p/2$, $\omega_0 = 20\omega_p$; $\lambda_p = 2\pi c/\omega_p$ is the plasma wavelength), and $\beta_0/\omega_p \sim \mathcal{O}(10^{-2})$, $(L_{in}/L_0)^2 \sim 0.37$, in this case the expression for the pulse length (equation (5)) simplifies to

$L = L_0(1 - 2\beta_0 t \omega_p^2 / \omega_0^2)$, which predicts that the positive (negative) frequency chirp compresses (stretches) the laser pulse as it propagates through the plasma. This can be interpreted by investigating the dynamics of different laser photons. For $\beta_0 > 0$ ($\beta_0 < 0$), the photons located at the front move slower (faster) than the photons located at the back (front) of the laser. Thus, the distance between the laser photons decreases (increases) as the laser propagates, and laser length thus decreases (increases).

In order to investigate further the role of the frequency chirp in the laser pulse length evolution, 1D OSIRIS PIC simulations [31] were performed. The simulation uses a moving window that travels at c, with length $30\,c/\omega_p$, and is divided into 3000 cells, with 500 particles per cell. The length of the plasma is $1000\,c/\omega_p$, and the ions form an immobile neutralizing fluid background. In this section, the role of the chirp is identified by keeping the laser length, a_0, and ω_0/ω_p constant regardless of the amount of chirp used. In section 4, studies are shown, where we change the pulse length and the vector potential of the laser consistently with its chirp.

The prediction for longitudinal compression (equation (5)) is in good agreement with the simulations, as illustrated in figure 1. Figure 1(a) uses a laser with $a_0 = 0.05$, $\omega_0/\omega_p = 20$ and $L_0 = 3\,c/\omega_p$, thus exciting linear plasma waves. The laser pulse compresses (stretches) linearly with time for positive (negative) frequency chirp. We note that in these conditions, and in comparison to the scenarios where $\beta_0 \neq 0$, the pulse length remains constant during the laser propagation for $\beta_0 = 0.0\omega_p$ (if dispersion effects are neglected). This thus indicates that the ponderomotive and relativistic nonlinearities cancel, confirming that the pulse compression is essentially determined by the initial frequency chirp. Figures 1(c)–(e) show the Wigner transform [35, 36], and average wavenumber distribution ($\langle k \rangle$) within a chirped laser pulse with $\beta_0 = 0.05\,\omega_p$ at $\omega_p(t) = 0$, $\omega_p t = 500$ and $\omega_p t = 1000$. The variation in average wavenumber is linear within the pulse until $\omega_p t \sim 500$, and varies as $\langle k \rangle = k_0(1 + 2\beta\xi)$, where $\beta = \beta_0 = 0.05\omega_p$ at $\omega_p t = 0$ and $\beta \approx \beta_0(L/L_0) = 0.057\omega_p$ at $\omega_p t = 500$. For time $\omega_p t > 1000$, $\langle k \rangle$ does not change linearly within the laser pulse. The laser evolution cannot be predicted by the theory discussed here for $\omega_p t > 1000$, since a nonlinear mechanism such as self-steepening [27] starts to be relevant.

Figure 1(b) shows the evolution of the laser length using $a_0 = 2.0$ for various frequency chirps ranging from $\beta_0 = -0.05\,\omega_p$ to $0.05\,\omega_p$. In this particular case, pulse compression is observed for the range of frequency chirps $\beta_0 \geqslant -0.05\,\omega_p$; however, the compression was relatively stronger for positively chirped pulses. At higher intensities ($a_0 \sim 1$), in conditions where our analytical model is not valid, the two nonlinearities (ponderomotive and relativistic mass) do not cancel each other entirely, resulting in the net compression of the pulse [27], and including the contribution of frequency chirp will produce the effects as shown in figure 1(b).

In this section, we have shown that the initial frequency chirp can compress or stretch the laser pulse depending upon the sign of β_0. In the next section, we examine the effect of frequency chirp on the wakefield excitation in the linear regime due to the longitudinal bunching.

3. Wakefield excitation in the linear regime

The plasma density modulations driven by a linearly polarized laser with normalized vector potential $a_L = a_0 \times Z(z, t) \times \cos[\omega_0(1 + \beta\xi)\xi]$ are given by [7, 38]

$$\left(\frac{\partial^2}{\partial t^2} + \omega_p^2 \right) \frac{\tilde{n}}{n_0} = \frac{c^2}{2} \frac{\partial^2}{\partial \xi^2} |a_L^2|, \tag{6}$$
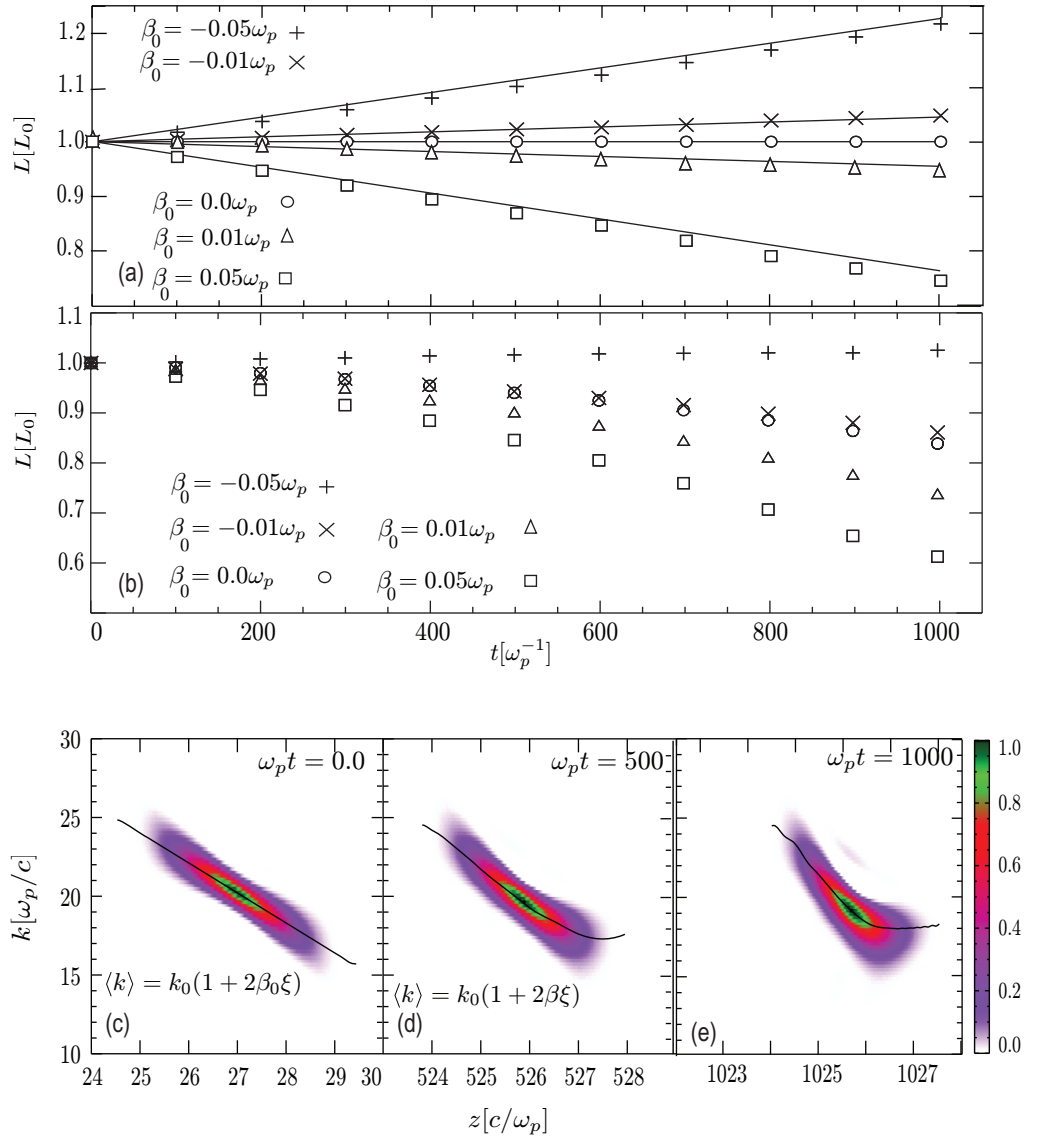
Figure 1. Effect of the initial laser frequency chirp on longitudinal bunching: (a) the variation of L (normalized by L_0) with time t (normalized by ω_p^{-1}) in the linear regime ($a_0 = 0.05$, $\omega_0/\omega_p = 20$, $L_0 = 3c/\omega_p$), and (b) the variation of L with time in the nonlinear regime ($a_0 = 2.0$, $\omega_0/\omega_p = 20$, $L_0 = 5c/\omega_p$) for various β_0, ranging from $-0.01\,\omega_p$ to $0.01\omega_p$. Solid lines in (a) show the theoretical prediction for the pulse length evolution with time for different chirps. Panels (c)–(e) plot the Wigner transform of the positively chirped laser ($\beta_0 = 0.05\,\omega_p$) used in the linear regime (a), and the solid lines represent the $\langle k \rangle$ distribution within the pulse at $\omega_p t = 0$, 500 and 1000, respectively.

where a_0 is the initial peak normalized vector potential, $Z(z, t)$ is the longitudinal profile of a_L, $\tilde{n}$ is the density modulation in the wake and n_0 is the initial homogeneous plasma density. Considering that the laser electric field in 1D is given by $\vec{E} = \hat{x} E_0 \exp[-\xi^2/(2L(t)^2)] \cos(\omega\xi)$,
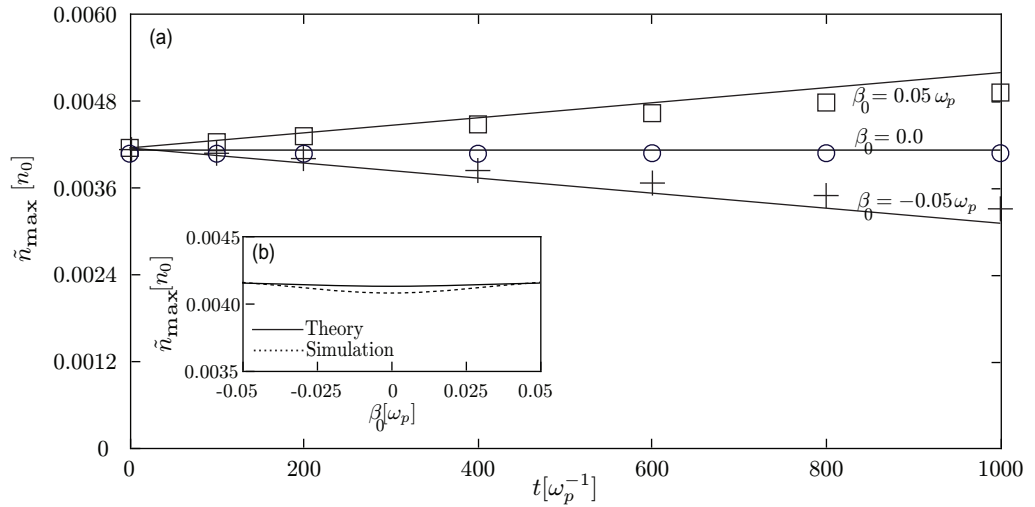
Figure 2. Evolution of peak plasma density (n_{max}) as a function of propagation distance for different chirps and using $a_0 = 0.05$, $\omega_0/\omega_p = 20$ and $L_0 = 3\,c/\omega_p$. (a) The simulation values of $\tilde{n}_{max}$ at different times for chirp coefficients $\beta = 0.0\,\omega_p$ are given by (○), $-0.05\,\omega_p$ by (+) and $0.05\,\omega_p$ (□). (b) A comparison of theory (dashed line) and the simulation (solid line) by plotting the $\tilde{n}_{max}$ normalized by n_0 with the frequency chirp coefficient β_0 (normalized by ω_p) at an early stage, neglecting the effect of pump evolution. Solid lines in (a) show the theoretical predictions.

then Z is given as

$$Z = \frac{1}{1 + \beta\xi} \sqrt{\frac{L_0}{L(t)}} \exp[-\xi^2/(2L(t)^2)], \tag{7}$$

where $L(t)$ is given by equation (5). Further assuming that $\beta L/c \ll 1$, the 1D solution for equation (6) is [7, 38]

$$\tilde{n} = \frac{1}{2\omega_p} \int_{-\infty}^{\xi} \sin\{\omega_p(\xi - \xi')\} \left[\frac{\partial^2}{\partial \xi^2} |a^2| \right]_{\xi = \xi'} d\xi'. \tag{8}$$

In order to directly compare the theoretical predictions of the plasma density modulations with the simulations, equation (8) was solved using the same laser pulse profile as that used in the simulations. In the simulations, we have used a Gaussian-like fifth-order symmetric polynomial profile defined as

$$Z = 10 f(z)^3 - 15 f(z)^4 + 6 f(z)^5, \tag{9}$$

where, for $-L_0 < z < 0$, $f(z) = (L_0 + z)/L_0$, and for $0 < z < L_0$, $f(z) = (L_0 - z)/L_0$. We have used the simulation parameters from section 2. Figure 2(b) shows the initial wakefield amplitude for different frequency chirps. For the typical values of βL_0 used in our simulations, no significant variation in the wake, at initial time, is observed with different βs; for example, for $\beta_0 = \pm 0.05\,\omega_p$, the wakefield amplitude changes by 1% of the wake amplitude driven by an un-chirped laser pulse. This is because, if we ignore the pulse length variation, the normalized peak laser vector potential is $a_L/a_{\beta=0} = 1/(1 - \beta_0^2 L_0^2/c^2) \simeq 1$, $a_{\beta=0}$ being the peak

laser vector potential for $\beta_0 = 0$, no significant change in the wakefield with frequency chirp can be expected. Figure 2(a) demonstrates, however, that the frequency chirp ($\beta_0 \geqslant 0.05\,\omega_p$) can significantly change the amplitude of the plasma wave during laser propagation. Since the laser pulse compresses or stretches according to the sign of β_0 (cf section 2), with increasing or decreasing laser vector potential, the amplitude of the plasma density modulation also changes accordingly. The evolution of the wakefield amplitude, plotted in figure 2(b), shows that this amplitude increases (decreases) for a positively (negatively) chirped pulse, as the laser peak vector potential increases (decreases). Inserting equation (5) into equation (10), the vector potential can be approximated as

$$a^2 \approx a_0^2(1 + 2\beta_0 t\omega_p^2/\omega_0^2)\exp[-\xi^2/L_0^2]/(1 + \beta_0\xi)^2, \tag{10}$$

which, using in equation (8), gives $\tilde{n} \approx (1 + 2\beta_0 t\omega_p^2/\omega_0^2)\tilde{n}_0$, where $\tilde{n}_0$ is the initial wake amplitude. Thus, the density perturbation depends upon the chirp as

$$\tilde{n}/\tilde{n}_0 - 1 \approx 2\beta_0\omega_p^2/\omega_0^2 t. \tag{11}$$

The theoretical estimates for the density modulations match with the simulation results as shown in figure 2.

In a transform-limited 20 fs Ti:sapphire laser pulse, the maximum chirp coefficient that can be introduced is around $\beta_0 \approx 1.0 \times 10^{12}\,\mathrm{s}^{-2} \sim 0.01\,\omega_p$ by stretching the pulse to ~ 28.3 fs, for $\omega_0 = 20\,\omega_p$. In such scenarios, the wake amplitude changes by only 0.5% at $\omega_p t = 1000$. Therefore, pulse compression, and hence the wakefield enhancement due to frequency chirp, play a significant role in LWFA for higher values of frequency chirp coefficients $\beta_0 \geqslant 0.05\,\omega_p$, which can be achieved by stretching a ~ 12 fs transform-limited laser pulse to a chirped ~ 18 fs laser pulse.

In the blowout regime, where the plasma dynamics is highly nonlinear, effects like self steepening and localized laser absorption also play a significant role in driving a nonlinear wake, and in self-injection. In such scenarios, frequency chirp may influence the laser etching rates, which can further affect the injection rates and beam characteristics. This will be analyzed in the following section.

4. Blowout regime

In order to investigate the role of laser frequency chirp in the blowout regime, a set of 3D PIC simulations were performed. For this purpose we consider a linearly polarized 350 mJ transform-limited laser with pulse duration 20 fs (full-width at half-maximum (FWHM) of the field) and 6 μm spot size, with the central laser wavelength $\lambda_0 = 800$ nm. In the simulation, these parameters are translated into a transform-limited pulse with $a_0 = 5.0$, central frequency $\omega_0 = 8\,\omega_p$, pulse length $L_0 = 5\,c/\omega_p$, transverse spot size $W_0 = 5\,c/\omega_p$ and Gaussian transverse field profile given as $\exp(-r^2/W_0^2)$, where r is the transverse coordinate, for a homogeneous plasma with plasma density $n_0 = 1.75 \times 10^{19}\,\mathrm{cm}^{-3}$. As the pulse is stretched, the maximum chirp coefficient $\beta_{\max} = c^2 \ln 2/L_{\mathrm{in}}^2$ can be obtained at $L = 1.414\,L_{\mathrm{in}}$ [37]. This corresponds to a chirp coefficient of $\beta_0 = 0.0055\,\omega_p$; the peak normalized vector potential is reduced to $a_0 = 4.23$. Adding this frequency chirp stretches the pulse to ~ 30 fs. To keep the pulse length and plasma wavelength ratio equivalent to the transform-limited laser case, i.e. $L = 5\,c/\omega_p$, the electron density is lowered to $n_0 = 8.77 \times 10^{18}\,\mathrm{cm}^{-3}$, which translates into $\omega_0 = 11.3\,\omega_p$ and $W_0 = 3.54\,c/\omega_p$ for a chirped pulse. For a negatively chirped pulse with $\beta = -0.0055\,\omega_p$,
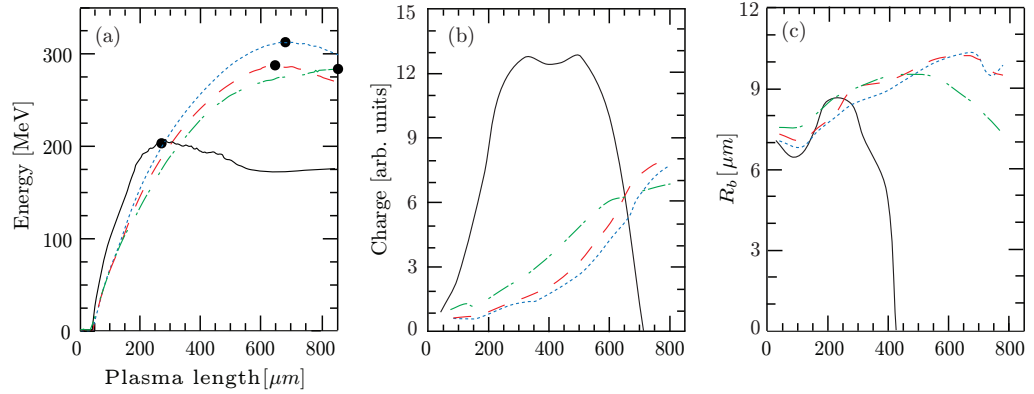
Figure 3. Time evolution of (a) peak energy, (b) total charge injected inside the first bubble and (c) bubble radius (R_b) in four scenarios (cases). Case (i): (solid line (black)) transform-limited pulse with $a_0 = 5.0$, $\omega_0 = 8\,\omega_p$, $W_0 = 5\,c/\omega_p$ and $L = 5\,c/\omega_p$. Case (ii): (dash-dot line (green)) the same transform-limited pulse with $a_0 = 5.0$, $\omega_0 = 11.3\,\omega_p$, $W_0 = 3.54\,c/\omega_p$ and $L = 3.54\,c/\omega_p$. Case (iii): (dashed line (red)) positively chirped laser pulse with $\beta = 0.0055\omega_p$, $a_0 = 4.23$, $\omega_0 = 11.3\,\omega_p$, $W_0 = 3.54\,c/\omega_p$ and $L = 5\,c/\omega_p$. Case (iv) (dotted line (blue)) negatively chirped pulse with $\beta = -0.0055\omega_p$, $a_0 = 5.0$, $\omega_0 = 11.3\,\omega_p$, $W_0 = 3.54\,c/\omega_p$ and $L = 5\,c/\omega_p$. Dark dots in figure 3(a) represent the time at which peak energy as well as peak efficiency is achieved in LWFA. The efficiencies for cases (i), (iii) and (iv) are the same, greater than the efficiency for case (ii) by $\sim 15\%$.

the rest of the laser simulation parameters are equivalent to the positively chirped pulse ($\beta = 0.0055\,\omega_p$) case. These chirps can be routinely introduced/controlled in the experiments with lasers [40]. In order to compare directly the effect of chirp on the LWFA, a simulation using the transform-limited pulse propagating in a plasma with density $n_0 = 8.77 \times 10^{18}\,\text{cm}^{-3}$ (the same as used with the chirped pulses) was also performed, using as simulation parameters $a_0 = 5$, $L_0 = 3.54\,c/\omega_p$, $W_0 = 3.54\,c/\omega_p$ and $\omega_0 = 11.3\,\omega_p$. The laser is initialized in a simulation window that moves with the speed of light, and with dimensions $30\,c/\omega_p \times 36\,c/\omega_p \times 36\,c/\omega_p$, divided into $1800 \times 180 \times 180$ cells. The 3D simulations used two particles per cell.

Figure 3 shows the variation of electron beam energy and total charge in the first bucket due to the introduction of frequency chirp in a transform-limited pulse in the 3D simulations. We discuss here results for four cases, (i) a transform-limited pulse with $a_0 = 5$, $\omega_0 = 8\,\omega_p$, $L_0 = 5\,c/\omega_p$ and $W_0 = 5\,c/\omega_p$; (ii) the same transform-limited pulse (but with plasma density the same as used with the chirped pulse) with $a_0 = 5$, $\omega_0 = 11.3\,\omega_p$, $L_0 = 3.54\,c/\omega_p$ and $W_0 = 3.54\,c/\omega_p$; (iii) a positively chirped pulse with $\beta = 0.0055\,\omega_p$, $a_0 = 4.23$, $\omega_0 = 11.3\,\omega_p$, $L_0 = 5\,c/\omega_p$ and $W_0 = 3.54\,c/\omega_p$; and (iv) a negatively chirped pulse with $\beta = -0.0055\,\omega_p$, $a_0 = 4.23$, $\omega_0 = 11.3\,\omega_p$, $L_0 = 5\,c/\omega_p$ and $W_0 = 3.54\,c/\omega_p$. Two scenarios are identified. Firstly, when the ratio of pulse duration to plasma wavelength is kept constant by changing the plasma density (cases (i), (iii) and (iv)); and secondly, when plasma density is kept the same (cases (ii), (iii) and (iv)). In the first scenario, for the chirped pulse (cases (iii) and (iv)) the peak energy

of the accelerated electrons reaches 1.5 times the peak energy that can be reached using the transform-limited pulse (case (i)) but on longer time scales (figure 3(a)). The higher peak energy for a chirped pulse is obtained at the expense of lower total charge (figure 3(b)) as compared to the transform-limited (un-chirped) laser pulse. The main reason behind these differences is the higher ω_0/ω_p, i.e. lower plasma density in the case of the chirped pulse. Since the laser group velocity (v_g), and hence the wake phase velocity v_ϕ, which play a key role in the self-trapping mechanisms in the LWFA [21, 24], is lower for larger densities, the trapping thresholds [7] in case (i) is relaxed as compared to the cases (ii), (iii) and (iv).

In the case of a transform-limited laser pulse (case (i)), the peak energy (200 MeV) is achieved after $\sim 200\,\mu$m. At $\sim 400\,\mu$m, the laser becomes pump-depleted, and a transition to the plasma wakefield accelerator (PWFA) was observed. Since the blowout radius is measured at the same longitudinal position in figure 3(c), it drops to zero when the laser pump depletes. Simulations show that self-injection still occurs when the wake is driven by the laser self-injected electrons, which increases the total charge of the beam at $\sim 500\,\mu$m. At $\sim 700\,\mu$m, the self-injected electrons can no longer sustain the wake, and are lost to the background plasma. The total acceleration length for LWFA in this case is $\sim 220\,\mu$m, which is three times smaller compared to the acceleration lengths observed for the chirped pulse. The dark dots in figure 3(a) represent the points where the peak energy is reached. The efficiency is similar for all three cases. For the chirped pulse the self-injection and acceleration process is relatively gradual compared to the un-chirped pulse. The amount of injected charge for the chirped pulse can reach up to 60% of the total charge obtained with the transform-limited pulse (case (i)).

In the second scenario (keeping the plasma density constant), the peak energy for the transform-limited pulse (case (ii)) is $\sim 15\%$ lower than in the case of a negatively chirped pulse (figure 3(a)), and with the total peak charge $\sim 16\%$ less than the charge obtained with the chirped pulse (figure 3(b)). Hence, using a chirped pulse in place of a transform-limited pulse results in better efficiency, as well as $\sim 25\%$ shorter acceleration lengths.

Within the chirped pulses, the positively chirped pulse provides higher (lower) charge (peak energy) as compared to the negatively chirped pulse (figure 3). Simulations suggested that the higher final electron energies in the case of a negatively chirped pulse are due to the fact that negatively chirped laser propagates with higher group velocities, followed by the bubble with a higher phase velocity. This increases the threshold for the initial γ of the electrons which can be trapped, reducing the number of electrons as well as electrons that can be accelerated to higher velocities. Beam loading effects [41] also play a significant role in reducing the wake field for the positively chirped pulse due to the higher charge self-injection, whereas for the negatively chirped pulse the beam loading effects are not significant due to relatively lower charge injection compared to the positively chirped pulse. These simulations showed that by adjusting the initial chirp of the laser pulse, the number of self-injected electrons and self-injected electron beam energy can be controlled. For the laser parameters discussed here, the difference in total charge for the two chirped cases ((iii) and (iv)) can reach up to 15%, and in peak energy 10% of the difference can be achieved. These results highlight some of the advantages of using chirped pulsed laser in LWFA.

According to section 3, the wake field amplitude is not significantly changed for the frequency chirp discussed here. We believe that it is the combined effect of longitudinal bunching as well as localized etching of the laser that leads to differences in LWFA by positively and negatively chirped pulse.
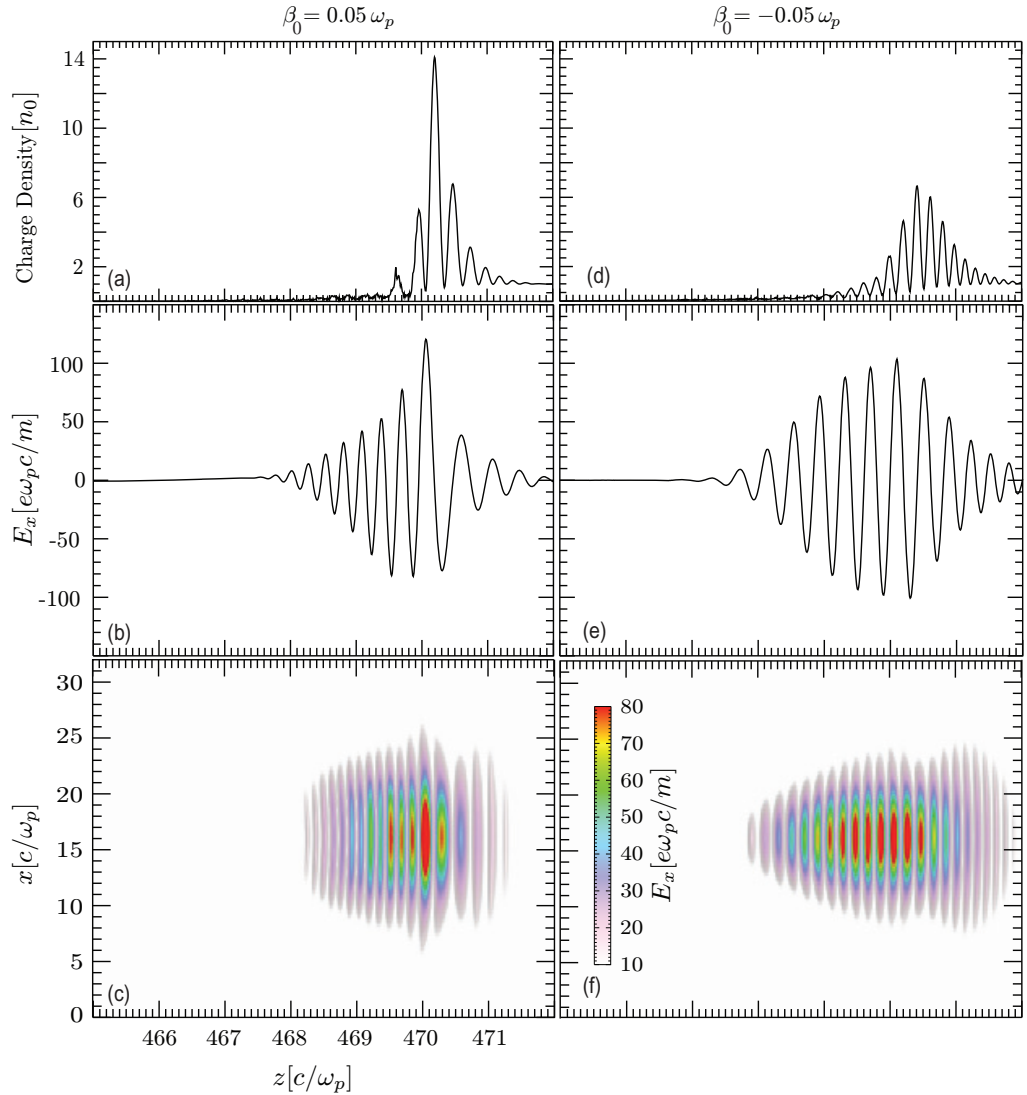
Figure 4. Effect of the frequency chirp on localized laser etching: (a), (d) line out of charge density on the axis at the front of the laser, (b), (e) line out of laser field on the axis and (c), (f) laser field (E_x) in the x–z plane at time $448.43/\omega_{\mathrm{p}}$ for $\beta = 0.05\,\omega_{\mathrm{p}}$ (a, b, c) and $\beta = -0.05\,\omega_{\mathrm{p}}$ (d, e, f), respectively.

Considering the effect of localized etching [42], the laser group velocity v_{g} is given by $v_{\mathrm{g}} = v_{\mathrm{g}}^{\mathrm{l}} - v_{\mathrm{etch}}$, where $v_{\mathrm{g}}^{\mathrm{l}} = c[1 - \omega_{\mathrm{p}}^2/(2\omega(\xi_{\mathrm{etch}})^2)]$ is the laser linear group velocity, $v_{\mathrm{etch}} = c\omega_{\mathrm{p}}^2/\omega(\xi_{\mathrm{etch}})^2$ is the etching velocity [42] and ξ_{etch} is the position of the localized etching within the laser in ξ coordinates. A positively chirped pulse, with a red shifted front, etches faster, and may thus propagate with lower group velocity, compared to a negatively chirped laser pulse. Furthermore, the phase velocity of the plasma wave (wake), propagating at the back of a laser, is roughly equal to the group velocity of the laser; thus, for a positively chirped laser pulse the wake phase velocity is lower compared to a bubble propagating behind a negatively chirped laser pulse. Electrons with a sufficiently high velocity in the forward direction (this velocity is roughly equal to the phase velocity of the bubble at the back) have higher probability of getting

trapped inside the bubble ([39] and the references therein), which means that the positively chirped laser pulse lowers the threshold for electron trapping by slowing down the wake. On the other hand, a negatively chirped laser pulse will have a higher group velocity, thus increasing the threshold for trapping.

To illustrate clearly the effect of positive and negative frequency chirps on localized etching and on laser self-guiding [39], in figure 4, we show the results of 3D PIC simulations for two linearly polarized laser pulses with $a_0 = 5.0$, with central frequency $\omega_0 = 20\omega_{\mathrm{p}}$, pulse length $L_0 = 3c/\omega_{\mathrm{p}}$, transverse spot size $W_0 = 4.5c/\omega_{\mathrm{p}}$ and $\beta = \pm 0.05\omega_{\mathrm{p}}$. We have exaggerated the chirp such that effects attributed to the chirp are clearly visible. Since for $\beta > 0$ the laser intensity is higher at the front than when $\beta < 0$, a sharper density spike is formed at the front of the laser for $\beta > 0$ (figures 4(a) and (d)), which leads to a stronger localized pump depletion (figures 4(b)–(f)). For the negatively chirped pulse considered in the simulations, the density spikes are not sharp, so the localized etching is either absent, or very weak, as compared to the positively chirped pulse. Thus, positively chirped lasers may also relax the self-guiding conditions for stable laser propagation in the blowout regime. These results indicate that the variation in laser group velocity and localized pump depletion, due to the initial laser frequency chirp, may impact the rates at which self-injection occur and the number of self-trapped particles. For the parameters considered in figure 3 (cases (ii) and (iii)), we observe the effect of chirp sign (positive or negative) on localized laser etching; however, and for realistic chirps, the effects are not as strong as shown in figure 4, since the amount of frequency chirp used in the laser for figure 4 is five times as high as the amount of frequency chirp used in the laser for figure 3.

5. Conclusions

In conclusion, we have examined the effect of the frequency chirp on LWFA. In the linear regime, a positive (negative) frequency chirp compresses (stretches) the laser pulse, resulting in enhanced (reduced) wakefield amplitude with time due to dispersive effects. In the blowout regime and using the chirps that can be routinely introduced in the experiments, simulations show that negatively chirped lasers can provide higher peak energies to the self-injected electrons in comparison to un-chirped lasers. Moreover, chirped laser pulses can also lead to a higher number of self-injected electrons. In addition, the laser group velocity, and thus the wake phase velocity, is lower (higher) when the laser frequency is lower (higher) at the front of the laser due to positive (negative) frequency linear chirp, which then influences the rate at which self-injection occurs and the number of self-injected electrons, providing extra control over the self-injection process in LWFA.

Acknowledgments

References

[1] Blumenfeld I *et al* 2007 *Nature* **445** 741
[2] Faure J *et al* 2006 *Nature* **444** 737
[3] Geddes C G R *et al* 2004 *Nature* **431** 538
[4] Martins S F *et al* 2010 *Nature Phys.* **6** 311
[5] Martins S F *et al* 2010 *Phys. Plasmas* **17** 056705
[6] Tajima T and Dawson J M 1979 *Phys. Rev. Lett.* **43** 267
[7] Esarey E and Sprangle P 1996 *IEEE Trans. Plasma Sci.* **24** 252
[8] Pukhov A and Meyer ter Vehn J 2002 *Appl. Phys. B: Lasers Opt.* **74** 355
[9] Lu W *et al* 2006 *Phys. Rev. Lett.* **96** 165002
[10] Mangles S P D *et al* 2004 *Nature* **431** 535
[11] Leemans W P *et al* 2006 *Nature Phys.* **2** 696
[12] Clayton C E *et al* 2010 *Phys. Rev. Lett.* **105** 105003
[13] Whittum D, Sessler A and Dawson J 1990 *Phys. Rev. Lett.* **64** 2511
[14] Wang S *et al* 2004 *Phys. Rev. Lett.* **88** 135004
[15] Kiselev S, Pukhov A and Kostyukov I 2004 *Phys. Rev. Lett.* **93** 135004
[16] Kneip S *et al* 2010 *Nature Phys.* **6** 980
[17] Schroeder C B, Fawley W M, Esarey E and Leemans W P 2006 *Proc. FEL 2006* p 455 JACoW
     (http://www.jacow.org)
     Grüner F *et al* 2007 *Appl. Phys.* B **86** 431
[18] Esarey E *et al* 2002 *Phys. Rev.* E **65** 056505
[19] Geddes C G R *et al* 2008 *Phys. Rev. Lett.* **100** 215004
[20] Faure J *et al* 2010 *Phys. Plasmas* **17** 083107
[21] Vieira J *et al* 2011 *Phys. Rev. Lett.* **106** 225001
[22] Kotaki H *et al* 2009 *Phys. Rev. Lett.* **103** 194803
[23] Davoine X *et al* 2009 *Phys. Rev. Lett.* **102** 065001
[24] Pak A *et al* 2010 *Phys. Rev. Lett.* **104** 025003
[25] Berezhiani V I and Murusidze I G 1992 *Phys. Scr.* **45** 87
[26] Faure J *et al* 2001 *Phys. Rev.* E **63** 065401
[27] Vieira J, Fiuza F, Silva L O, Tzoufras M and Mori W B 2010 *New J. Phys.* **12** 045025
     Tsung F *et al* 2002 *Proc. Natl Acad. Sci. USA* **99** 29
[28] Dodd E S and Umstadter D 2001 *Phys. Plasmas* **8** 3531
[29] Schroeder C B *et al* 2003 *Phys. Plasmas* **10** 285
[30] Leemans W P *et al* 2002 *Phys. Rev. Lett.* **89** 174802
[31] Fonseca R A *et al* 2002 *Lecture Notes in Computer Science* vol 2331/2002 (Berlin: Springer)
     Fonseca R A *et al* 2008 *Plasma Phys. Control. Fusion* **50** 124034
[32] Ren C *et al* 2001 *Phys. Rev.* E **63** 026411
[33] Mori W B 1997 *IEEE J. Quantum Electron.* **33** 1942
[34] Decker C D and Mori W B 1994 *Phys. Rev. Lett.* **72** 490
[35] Silva L O and Mendonça J T 1998 *Phys. Rev.* E **57** 3423
[36] Serimaa O T, Javanainen J and Varr S 1986 *Phys. Rev.* A **33** 2913
[37] Silvestri S D, Laporta P and Svelto O 1984 *IEEE J. Quantum Electron.* **QE-20** 533
[38] Keinigs R and Jones M E 1987 *Phys. Fluids* **30** 252
[39] Lu W *et al* 2007 *Phys. Rev. ST Accel. Beams* **10** 061301
[40] Hong K-H *et al* 2002 *Appl. Phys.* B **74** (suppl) S2310
[41] Tzoufras M *et al* 2008 *Phys. Rev. Lett.* **101** 145002
[42] Decker C D *et al* 1996 *Phys. Plasmas* **3** 2047